

TRACING STAR FORMATION WITH NON-THERMAL RADIO EMISSION

J. SCHOBER

Nordita, KTH Royal Institute of Technology and Stockholm University,
Roslagstullsbacken 23, 10691 Stockholm, Sweden

D. R. G. SCHLEICHER

Departamento de Astronomía, Facultad Ciencias Físicas y Matemáticas, Universidad de Concepción,
Av. Esteban Iturra s/n Barrio Universitario, Casilla 160-C, Concepción, Chile

R. S. KLESSEN

Universität Heidelberg, Zentrum für Astronomie, Institut für Theoretische Astrophysik,
Albert-Ueberle-Strasse 2, D-69120 Heidelberg, Germany and
Universität Heidelberg, Interdisziplinäres Zentrum für Wissenschaftliches Rechnen,
Im Neuenheimer Feld 205, D-69120 Heidelberg, Germany*Draft version November 28, 2016*

ABSTRACT

Understanding the evolution of galaxies and in particular their star formation history is a central challenge of modern cosmology. Future radio telescopes will be able to observe galaxies at extremely high redshifts and make it possible to constrain theoretical scenarios of galaxy evolution. Along these lines, it is of crucial importance to have theoretical tools for analyzing the observational data from future radio surveys. In this paper we present a physical model that explains the correlation between the non-thermal radio flux and the star formation rate (SFR). This model is based on an analytical description of the steady-state cosmic ray spectrum including energy losses by ionization, bremsstrahlung, inverse Compton scattering, synchrotron radiation, and galactic outflows. As cosmic rays are produced in supernova remnants, their injection rate is proportional to the supernova rate and thus also to the SFR. When these highly energetic charged particles travel in the magnetized interstellar medium they emit non-thermal synchrotron radiation. As a result there is a relation between the SFR and the non-thermal radio emission. A crucial point is that synchrotron emission can be absorbed again by the free-free mechanism. This suppression becomes stronger with increasing number density of the gas, more precisely of the free electrons, and with decreasing frequency. We present an estimate of the critical frequency above which radio emission can be used as a tracer for the SFR. If the observed galaxy is redshifted, this critical frequency moves along with other spectral features to lower values in the observing frame. The method can therefore be successfully applied at high redshift. However, for high redshift, i.e. $z \gtrsim 5$, and observations at high radio frequency bands, i.e. $\nu \gtrsim 50$ GHz, special caution should be paid, as the observed flux might be dominated by free-free emission or the thermal contribution.

1. INTRODUCTION

Theory suggests that the first galaxies have formed at redshifts z between 10 and 15 in atomic cooling halos and developed further through accretion and mergers (Bromm and Yoshida 2011; Conselice 2014; Madau and Dickinson 2014; Somerville and Davé 2015). The evolution of a galaxy is influenced by various physical processes like turbulence (e.g. Wise *et al.* 2008; Greif *et al.* 2008), feedback from stars (e.g. Ceverino and Klypin 2009) and active galactic nuclei (e.g. Bower *et al.* 2006; Hopkins *et al.* 2016), merger and accretion rates (e.g. Lotz *et al.* 2008), and possibly also magnetic fields (Pakmor and Springel 2013). While the study of galaxy evolution has been a mostly theoretical discipline, modern telescopes have provided a deep look into the highly redshifted Universe. In the *Hubble Ultra Deep Field* galaxies have been detected at redshifts of approximately 8 and above (Bouwens *et al.* 2010; McLure *et al.* 2010; Bouwens *et al.* 2011) and owing to the gravitational lens-

ing effect, detailed studies are possible for single high- z galaxies (Ivison *et al.* 2010). Several surveys have been performed at radio wavelengths (Garrett 2002; Gruppi *et al.* 2003; Appleton *et al.* 2004; Jarvis *et al.* 2010; Sargent *et al.* 2010; Bourne *et al.* 2011) with the goal of identifying radio counterparts to infrared sources. These surveys will soon be complemented by the new generation of radio telescopes, which will perform exhaustive surveys of the 'cosmic dawn'. The data sets from the *LOw Frequency ARray*¹ (LOFAR) and the *Square Kilometer Array*² will be extremely important to constrain theoretical models for galaxy evolution. Hence it is crucial to develop theoretical tools for interpreting spectra as well as fluxes at single frequencies. In this paper we explore the possibility to determine the star formation rate from the galactic radio flux.

The origin of non-thermal radio emission from star-forming galaxies are synchrotron losses of highly ener-

¹ <http://www.lofar.org/>² <https://www.skatelescope.org/>

getic charged particles, so-called cosmic rays, that spiral around magnetic field lines (Blumenthal and Gould 1970; Longair 2011). The main source of galactic cosmic rays are likely shock fronts in supernova remnants, where charged particles undergo first-order Fermi acceleration (Bell 1978a,b; Drury 1983; Schlickeiser 2002). As the rate of supernovae is related to the rate at which stars form, one can expect a connection between galactic synchrotron emission and the star formation rate (SFR) (Condon 1992). This coupling is reflected in the FIR-radio correlation which has been observed in the local Universe (Niklas and Beck 1997; Yun *et al.* 2001) and seems to hold also up to at least intermediate redshifts (Jarvis *et al.* 2010; Sargent *et al.* 2010; Bourne *et al.* 2011). The physical interpretation of this correlation is based on star formation, which is related to cosmic rays, and thus synchrotron emission, as well as to FIR emission, which originates from dust heated by stellar UV radiation (Bell 2003; Groves *et al.* 2003; Lacki *et al.* 2010; Lacki and Thompson 2010; Schleicher and Beck 2013, 2016; Schober *et al.* 2016). When using non-thermal radio emission as a tracer for the SFR, one needs to be particularly careful at low frequencies, where synchrotron emission gets exponentially suppressed by free-free absorption. This is a consequence of the frequency dependency of the optical depth τ_{ff} . In fact, below a critical frequency ν_{crit} τ_{ff} becomes larger than one and hence the medium becomes optically thick (Schober *et al.* 2016). As a result there is no correlation of non-thermal radio emission and the SFR below ν_{crit} . This frequency depends strongly on the gas density and the ionization degree in the galaxy. With LOFAR surveys are planned between the key frequencies 15 and 200 MHz where free-free absorption can play a crucial role. SKA will be operating at higher frequencies. Surveys with the SKA are planned at several GHz where the method presented in this paper should be applicable.

One goal of the future deep surveys is to measure the typical galactic SFR as a function of redshift. Several tracers of the star formation rate have been suggested in the literature all across the electromagnetic spectrum (Hao *et al.* 2011; Murphy *et al.* 2011; Kennicutt and Evans 2012). Most common are the FIR continuum flux, the 60 μm flux, the $\text{H}\alpha$ flux, and the UV flux. However, in surveys with the SKA sources will be detected for which only radio fluxes are available, making a radio calibration of the SFR necessary. Young galaxies typically have higher SFRs (Madau *et al.* 1998) and have higher mean gas densities. With the free-free processes being sensitive to the gas density, we expect much stronger absorption in the early Universe. On the other hand, the critical frequency below which synchrotron emission is absorbed shifts to lower values in the observed frame as redshift increases. As a result, a galaxy at $z = 0$ for which non-thermal radio emission cannot be used for estimating the SFR, can be suitable for this method at high redshift. In this paper we present an analytical model for the radio emission of galaxies. The description of cosmic rays includes a source term related to the supernova rate and several energy loss channels. Free-free emission and absorption depend strongly on the optical depth which is frequency dependent and a function of gas density and the ionization degree. We use our model to derive ν_{crit} below which synchrotron emission is suppressed for dif-

ferent types of star-forming galaxies. The correlation between the radio luminosity at various fixed frequencies and the SFR is calculated and explored for a large parameter space. Finally, we employ our model to high redshifts and then draw our conclusions.

2. PHYSICAL MODEL FOR NON-THERMAL RADIO EMISSION

2.1. Properties of cosmic ray electrons

Supernova remnants are most likely the birthplace of galactic cosmic rays, where charged particles gain relativistic energies through first order Fermi acceleration in shock fronts (Bell 1978a,b; Drury 1983; Schlickeiser 2002). The result of this process is a power law distribution in energy that is observed over more than ten orders of magnitude (Hillas 2006). We concentrate here on the cosmic ray electrons, as they are responsible for the largest contribution to the synchrotron emission due to their low mass. Shock acceleration leads to the following injected energy of cosmic ray electrons Q_e as a function of the Lorentz factor γ

$$Q_e(\gamma) = Q_{e,0} \gamma^{-\chi}. \quad (1)$$

The power law index χ has a typical value between 2.1 and 2.3 (Bogdan and Völk 1983) and we choose a value of $\chi = 2.2$ for this study.

In addition to primary e^\pm cosmic rays from supernovae, secondaries are produced from cosmic ray protons that decay into pions which in turn decay into e^\pm . For modelling the spectral energy distribution of e^\pm we follow the work of Lacki and Beck (2013) that has also been described in Schober *et al.* (2016). Taking both contributions into account, the normalization of the spectrum (1) is

$$Q_{e,0} = \frac{20^{2-\chi}}{6} \frac{f_\pi}{f_{\text{sec}}} \left(\frac{m_p}{m_e} \right)^\chi m_e c^2 Q_{p,0}. \quad (2)$$

Here $f_\pi \approx 0.4$ is the fraction of protons that decay into pions, $f_{\text{sec}} \approx 0.7$ is the ratio of secondary and total cosmic ray e^\pm , m_p and m_e are the masses of protons and electrons, and c is the speed of light. The normalization of the proton injection spectrum $Q_{p,0}$ can be directly related to the supernova rate \dot{N}_{SN} via

$$Q_{p,0} = \frac{\xi E_{\text{SN}} \dot{N}_{\text{SN}} (\chi - 2)}{m_p c^2 \gamma_{p,0}^{2-\chi}}, \quad (3)$$

where $\xi \approx 0.1$ is the fraction of the supernova energy $E_{\text{SN}} \approx 10^{51}$ erg that is converted into kinetic energy of cosmic rays (Dorfi 2000). The Lorentz factor $\gamma_{p,0} = 10^9 \text{ eV}/(m_p c^2) \approx 1$ marks the low energy end of the cosmic ray proton spectrum.

When traveling through the interstellar medium, cosmic rays lose energy continuously. The total number $N_e(\gamma)$ of e^\pm can be described as

$$\frac{\partial N_e(\gamma)}{\partial t} = Q_e(\gamma) + \frac{d}{d\gamma} \left[\frac{\gamma}{\tau_e(\gamma)} N_e(\gamma) \right], \quad (4)$$

where the energy losses are determined by the cooling timescale τ_e . At steady state we find

$$N_e(\gamma) = \frac{Q_e(\gamma) \tau_e(\gamma)}{\chi - 1}. \quad (5)$$

The different energy loss channels are: ionization (ion), bremsstrahlung (brems), inverse Compton scattering (IC), synchrotron emission (synch), and galactic outflows (wind). The individual timescales can be summarized as

$$\tau_{\text{ion}} = \frac{\gamma}{2.7 c \sigma_{\text{T}} (6.85 + 0.5 \ln \gamma) n}, \quad (6)$$

$$\tau_{\text{brems}} = 3.12 \times 10^7 \text{ yr} \left(\frac{n}{\text{cm}^{-3}} \right)^{-1}, \quad (7)$$

$$\tau_{\text{IC}} = \frac{3 m_e c}{4 \sigma_{\text{T}} u_{\text{ISRF}} \gamma}, \quad (8)$$

$$\tau_{\text{synch}} = \frac{3 m_e c}{4 \sigma_{\text{T}} u_B \gamma}, \quad (9)$$

$$\tau_{\text{wind}} = \frac{H}{v_{\text{wind}}}. \quad (10)$$

and result in the total cooling timescale

$$\tau_e = \left(\tau_{\text{ion}}^{-1} + \tau_{\text{brems}}^{-1} + \tau_{\text{IC}}^{-1} + \tau_{\text{synch}}^{-1} + \tau_{\text{wind}}^{-1} \right)^{-1}. \quad (11)$$

Here $\sigma_{\text{T}} \approx 6.65 \times 10^{-25} \text{ cm}^2$ is the Thomson cross section, $u_B = B^2/(8\pi)$ is the energy density of the magnetic field B , u_{ISRF} is the energy density of the interstellar radiation field, n is a gas density, H is the galactic scale height, v_{wind} the velocity of the galactic wind γ is the e^\pm Lorentz factor.

2.2. Synchrotron emission in a galactic magnetic field

In the presence of a magnetic field, cosmic rays perform spiral motions and hence are constantly accelerated. A single electron with a Lorentz factor γ results in the spectral power

$$L_{\text{synch},\nu,\gamma}(\nu, \gamma) = \frac{\sqrt{3} e^3 B}{m_e c^2} \frac{\nu}{\nu_c(\gamma)} \int_{\nu/\nu_c(\gamma)}^{\infty} K_{5/3}(x) dx, \quad (12)$$

where $K_{5/3}(x)$ is the modified Bessel function of second kind and $\nu_c(\gamma) = 3\gamma^2 e B/(4\pi c m_e)$ (see e.g. the review by Blumenthal and Gould 1970).

To find the synchrotron emission $L_{\nu,\text{synch}}$ produced from the full population of cosmic rays one has to integrate over the cosmic ray distribution, i.e.

$$L_{\text{synch},\nu}(\nu) = \int_{\gamma_{e,0}}^{\infty} L_{\text{synch},\nu,\gamma}(\nu, \gamma) N_e(\gamma) d\gamma \times \int N(\alpha) (\sin(\alpha))^{(\chi+1)/2} d\Omega_\alpha. \quad (13)$$

The last integral over the pitch angle Ω_α is roughly 8.9 for a cosmic ray spectrum with a slope of $\chi = 2.2$ and the lower limit of the γ integration is $\gamma_{e,0} = 10^7 \text{ eV}/(m_e c^2) \approx 20$.

We note that the synchrotron luminosity $L_{\text{synch},\nu}$ is directly proportional to the supernova rate \dot{N}_{SN} , which determines the total number of cosmic rays (see equation 3). As the supernova rate is correlated with the star formation rate, synchrotron emission can be used to estimate a galaxy's SFR.

2.3. Free-free emission and absorption

At low frequencies and high gas densities, the interstellar medium is optically thick and synchrotron emission, holding the information about the SFR, is absorbed. The optically thick regime is characterized by an optical depth τ_{ff} larger than 1. The value of τ_{ff} depends on the electron temperature T_e , the emission measure EM , and the frequency ν :

$$\tau_{\text{ff}}(n, \nu) = 0.082 \left(\frac{T_e}{\text{K}} \right)^{-1.35} \left(\frac{EM(n)}{\text{cm}^{-6} \text{ pc}} \right) \times \left(\frac{\nu}{10^9 \text{ Hz}} \right)^{-2.1}, \quad (14)$$

with

$$EM(n) \approx n_e(n)^2 H f_{\text{fill}}^{-1}. \quad (15)$$

The number density of the free electrons n_e can be related to the gas density via the ionization degree f_{ion} : $n_e = f_{\text{ion}} n$. The filling factor f_{fill} describes the clumping of the medium (Ehle and Beck 1993; Berkhuijsen *et al.* 2006; Beck 2007). The critical frequency ν_{crit} at which $\tau_{\text{ff}} = 1$, determining the transition from the optically thin to optically thick regime, is

$$\frac{\nu_{\text{crit}}}{10^9 \text{ Hz}} = \left(0.082 \left(\frac{T_e}{\text{K}} \right)^{-1.35} \left(\frac{EM(n)}{\text{cm}^{-6} \text{ pc}} \right) \right)^{1/2.1}. \quad (16)$$

In addition, we also expect a positive contribution to the radio spectrum from free-free emission. It can be estimated as

$$L_{\nu,\text{ff}}(\nu) = 2 k T_e c^{-2} \Delta A (1 - e^{-\tau_{\text{ff}}}) \nu^2. \quad (17)$$

The parameter ΔA is the surface area of the galaxy which depends of course on the galaxy's size as well as on its orientation along the line of sight. With a scaling proportional to ν^2 the free-free emission affects the radio spectrum mostly at high frequencies.

The total spectral radio emission including both, synchrotron emission and free-free effects, is then given as

$$L_\nu(\nu) = L_{\nu,\text{synch}}(\nu) e^{-\tau_{\text{ff}}(\nu)} + L_{\nu,\text{ff}}(\nu). \quad (18)$$

The total luminosity at a fixed frequency ν_0 can be estimated as $\nu_0 L_\nu(\nu_0)$.

3. RADIO LUMINOSITY IN THE LOCAL UNIVERSE

3.1. Basic assumptions, fiducial models, and parameter ranges

Our model for non-thermal radio emission includes several free parameters which vary in different individual star-forming galaxies. A list containing the typical range of all the free parameters is presented in Table 1. We distinguish here two different cases: a normal star-forming disk galaxy based on the Milky Way and a starburst galaxy based on M 82. The fiducial values of the free parameters are listed in the brackets in Table 1.

For determining the synchrotron luminosity the value of the magnetic field strength B is crucial. The total magnetic field observed in spiral galaxies is typically $B = 9 \pm 2 \mu\text{G}$ (Beck 2016), although there are also reports of nearby bright galaxies with $B = 17 \pm 3 \mu\text{G}$ (Fletcher

Table 1
Parameter range and fiducial values

parameter	abbreviation	normal star-forming galaxy (Milky Way)	starburst core (M 82)
magnetic field strength [μG]	B (B_0)	1 – 20 (10)	10 – 100 (50)
star formation rate [$M_\odot \text{ yr}^{-1}$]	\dot{M}_\star ($\dot{M}_{\star,0}$)	0.1 – 10 (2)	10 – 500 (10)
gas density [cm^{-3}]	n (n_0)	0.1 – 10 (2)	10 – 1000 (300)
intrinsic ISRF [erg cm^{-3}]	u_{int} ($u_{\text{int},0}$)	$10^{-13} - 10^{-11}$ (10^{-12})	$10^{-10} - 10^{-8}$ (10^{-9})
scale height [pc]	H (H_0)	250 – 1000 (500)	100 – 400 (200)
wind velocity [km s^{-1}]	v_{wind} ($v_{\text{wind},0}$)	1 – 100 (50)	10 – 500 (230)
electron temperature [K]	T_e ($T_{e,0}$)	$5 \times 10^3 - 1.5 \times 10^4$ (10^4)	$2.5 \times 10^3 - 10^4$ (5×10^3)
ionization degree	f_{ion} ($f_{\text{ion},0}$)	0.05 – 0.2 (0.1)	0.05 – 0.2 (0.1)
filling factor	f_{fill} ($f_{\text{fill},0}$)	0.1 – 0.3 (0.2)	0.1 – 0.3 (0.2)

Note. — The ranges of the different free parameters we are covering with our model for a normal star-forming galaxy and a starburst galaxy. Fiducial values (indicated by an index "0") for the Milky way and M 82 are given in brackets.

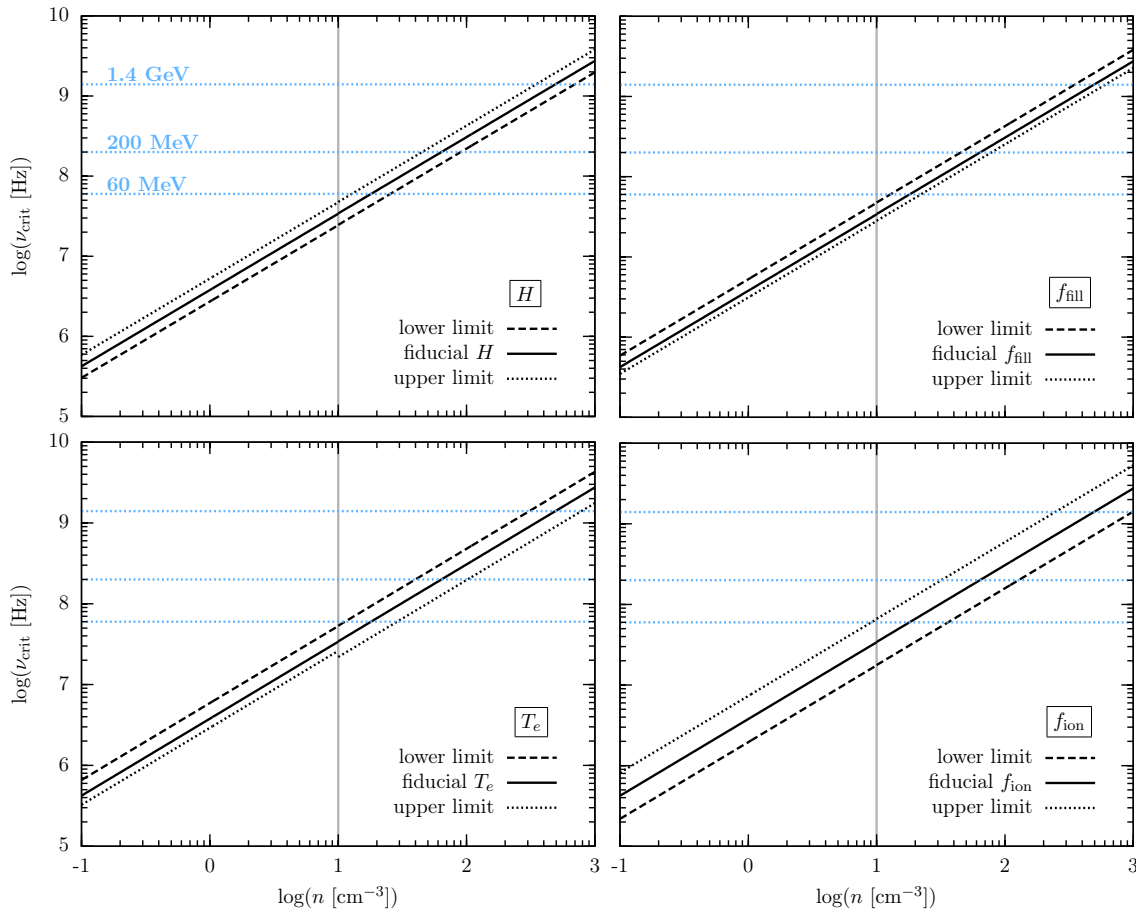


Figure 1. The critical frequency ν_{crit} that is defined via $\tau_{\text{ff}}(\nu_{\text{crit}}) \equiv 1$ as a function of gas density n . We test the dependency on the scale height H (top left panel), the filling factor f_{fill} (top right panel), the electron temperature T_e (lower left panel), and the ionization degree f_{ion} (lower right panel). The vertical gray line marks the transition from the normal galaxy model to the starburst model where densities are higher.

2010). Gas-rich galaxies with high star formation rates have considerably higher field strengths. Beck (2016) gives a typical value of $B = 20 - 30 \mu\text{G}$. In starburst galaxies values of $50 - 100 \mu\text{G}$ are observed (Chyży and Beck 2004; Beck *et al.* 2005; Heesen *et al.* 2011; Adebahr *et al.* 2013).

The second crucial parameter for the total synchrotron emission is the number of cosmic rays. The cosmic ray

injection rate is proportional to the supernova rate \dot{N}_{SN} which in turn depends on the SFR \dot{M}_\star . The relation between \dot{N}_{SN} and \dot{M}_\star is influenced by the choice of the initial mass function which determines how many massive stars are forming. Assuming a Kroupa (2002) initial mass function and a mean mass of stars evolving into

supernovae of $\overline{M}_{\text{SN}} \approx 12.26 M_{\odot}$ we find

$$\dot{N}_{\text{SN}} = 0.156 \frac{\dot{M}_{\star}}{\overline{M}_{\text{SN}}}. \quad (19)$$

For this study we choose a SFR range between 0.1 and $10 M_{\odot}\text{yr}^{-1}$ for the normal star-forming galaxies and 10 to $10^3 M_{\odot}\text{yr}^{-1}$ for the starbursts.

Besides the injection, the continuous energy losses determine the steady state number of cosmic rays. The number density of the neutral gas plays here a crucial role. It has been shown that the average midplane density n decreases exponentially with the galactic radius (Kalberla and Dedes 2008). To simplify the calculation we adopt a single mean density of $n_0 = 2 \text{ cm}^{-3}$ for the Milky Way, but also study a broader range between 0.1 and 10 cm^{-3} for disk galaxies in general. Densities are much higher in starburst cores. For the case of M 82 Colbert *et al.* (1999) report a density of 250 cm^{-3} if an 35 Myr old instantaneous starburst is assumed, while the density can be considerably higher for other scenarios. We use here $n_0 = 300 \text{ cm}^{-3}$ as a fiducial value, but also consider a larger range of $10 - 10^3 \text{ cm}^{-3}$.

Losses by inverse Compton scattering are determined by the interstellar radiation field. In Table 1 we present the values of the intrinsic interstellar radiation field u_{int} , which refers to the thermal component of the radiation field that is typically related to the SFR. For starburst galaxies u_{int} is considerably higher ($u_{\text{int}} \approx 10^{-9} \text{ erg cm}^{-3}$ for M 82) than for example for galaxies with low SFRs ($u_{\text{int}} \approx 10^{-12} \text{ erg cm}^{-3}$ for the Milky Way, see e.g. Draine 2011). In addition, we also include the contribution from the cosmic microwave background (CMB). The latter has an energy density of $u_{\text{CMB},0} \approx 4.2 \times 10^{-13} \text{ erg cm}^{-3}$ at redshift $z = 0$, but becomes more important in the early Universe. The total interstellar radiation field in our model is calculated as

$$u_{\text{ISRF}} = u_{\text{int}} + u_{\text{CMB},0}(1+z)^4. \quad (20)$$

The galactic scale height H is important to estimate the losses by outflows (10) and additionally determines the emission measure (15). The thickness of a disk galaxy shows a correlation with its rotational velocity (Kregel *et al.* 2002). A typical mean value for the Milky Way is 500 pc (Kennicutt and Evans 2012; Rix and Bovy 2013), but we also consider a variation of this value by a factor of 2. For compact starburst cores we choose a value of 200 pc (de Cea del Pozo *et al.* 2009) and again a variation by a factor of 2. For the free parameter v_{wind} we refer to a numerical study of a galactic disk by Girichidis *et al.* (2016) which shows that the bulk of the outflow occurs at low velocities of $20 - 40 \text{ km s}^{-1}$. However they also observe a high velocity tail with a few 100 km s^{-1} . We choose for our Milky Way model a value of $v_{\text{wind},0} = 50 \text{ km s}^{-1}$ as a reasonable fiducial value. For M 82 an outflow velocity of 230 km s^{-1} has been observed (Walter *et al.* 2002). The free-free optical depth (14) depends on the electron temperature T_e which can be determined accurately from recombination lines at radio and millimeter wavelengths. Quireza *et al.* (2006) find for the Milky Way a gradient between 4000 to 13000 K with a mean of $T_{e,0} = 10^4 \text{ K}$. Dusty starburst have usually lower excitation temperatures than the Milky Way. For M 82 a value of

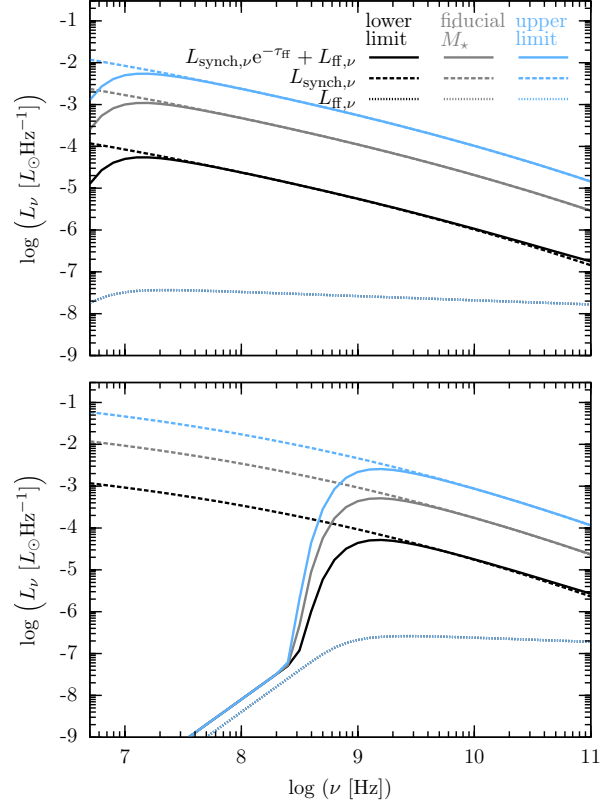


Figure 2. The spectral total radio luminosity $L_{\nu,\text{synch}}(\nu)e^{-\tau_{\text{ff}}(\nu)} + L_{\nu,\text{ff}}(\nu)$ (solid lines), the synchrotron component $L_{\nu,\text{synch}}(\nu)$ (dotted lines), and the free-free emission $L_{\nu,\text{ff}}(\nu)$. The fiducial model Milky Way model is shown in the left panel, the M 82 model in the right panel. The dependency on the SFR is tested for both cases.

$T_{e,0} = 5000 \pm 1000 \text{ K}$ has been observed (Puxley *et al.* 1989) which we adopt as our fiducial value. In addition the ionization degree, which determines the number density of free electrons, enters the calculation of τ_{ff} . A typical value for the warm interstellar medium is ten percent (Tielens 2005). Also the morphological structure of the gas distribution, described by the filling factor, affects the optical depth. For our fiducial model we use $f_{\text{fill}} = 0.3$ (Ehle and Beck 1993; Berkhuijsen *et al.* 2006; Beck 2007).

For this study the most interesting wavelength regime is where the emission is dominated by synchrotron radiation. We note, however, that the free-free flux scales as $S_{\nu} \propto \nu^{-0.1}$, while the synchrotron flux scales approximately as $S_{\nu} \propto \nu^{-0.6}$. Consequently, especially at high frequencies, the free-free emission might contribute significantly to the total observed flux. The equation for the free-free emission (17) includes another free parameter, the surface area of the galaxy ΔA . We employ here a fiducial value of 1 kpc^2 for the normal disk galaxies and a smaller value of 0.1 kpc^2 for the compact starbursts.

3.2. Using non-thermal radio emission to estimate the SFR

If synchrotron emission is not suppressed or the radio spectrum is contaminated by other sources, e.g. an active galactic nucleus, the non-thermal radio luminosity can be used to estimate the SFR. Strictly speaking, the free-free

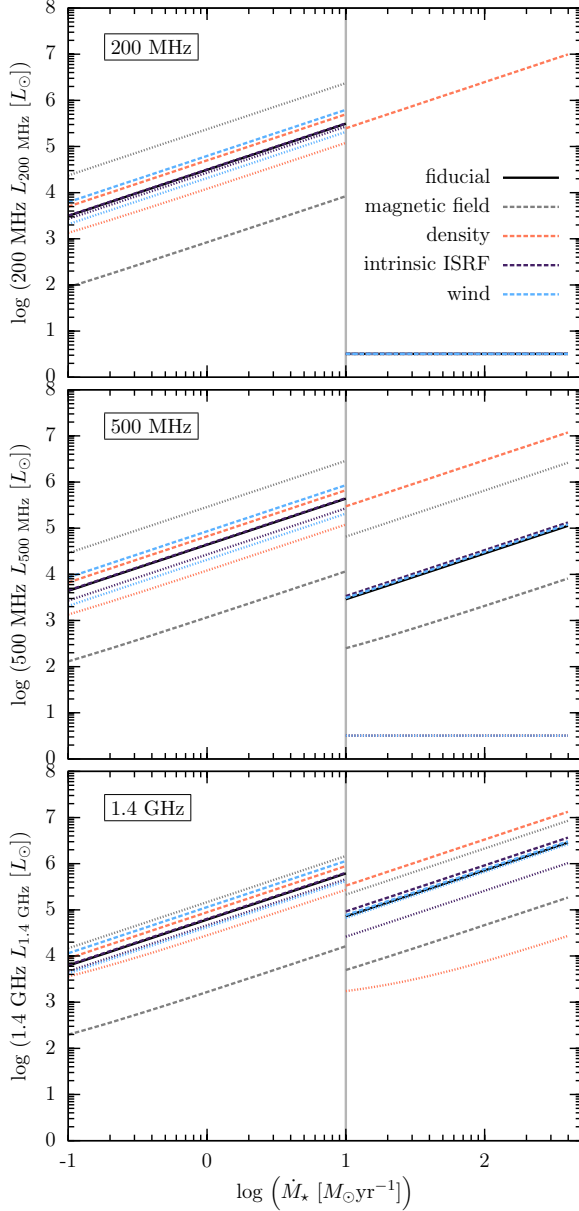


Figure 3. The total radio luminosity $\nu_0 L_\nu(\nu_0)$ as a function of the star formation rate. From left to right the observing frequencies are $\nu_0 = 60$ MHz, $\nu_0 = 200$ MHz, and $\nu_0 = 1.4$ GHz. The fiducial model is presented in black solid lines. Colored lines refer to the lower limit (dashed lines) and the upper limits (dotted lines) of the parameters listed in the plot legend. The parameter ranges are given in Table 1.

optical depth τ_{ff} needs to be less than one at the observed frequency, which is the case above the critical frequency ν_{crit} as given in equation (16). For our fiducial model based on the Milky Way we find a critical frequency of $\nu_{\text{crit}} \approx 7.3 \times 10^6$ Hz, while $\nu_{\text{crit}} \approx 8.7 \times 10^8$ Hz in the fiducial starburst case. We compute ν_{crit} as a function of gas density n and present the result in Figure 1, where we test the dependencies on the different free parameters. The gas density is separated in two regimes. At $n < 10 \text{ cm}^{-3}$ we use the model for a normal star-forming galaxy, for higher densities the one for the starburst. By the horizontal blue lines we indicate typical frequencies at which observations are performed. The strongest de-

pendency of ν_{crit} is on the density and the ionization degree. Figure 1 clearly shows that synchrotron emission is often suppressed in starburst galaxies. Especially at low observed frequencies, e.g. at 60 MHz, non-thermal radio emission is no tracer for the star formation rate.

The latter conclusion is confirmed by Figure 2 where we present the radio spectra for our two fiducial models. We plot the pure synchrotron emission $L_{\text{synch},\nu}$ as dotted lines, pure free-free emission $L_{\text{ff},\nu}$ as dashed lines, and the total radio luminosity as solid lines. In the upper panel the case of a Milky Way like galaxy is presented. Here the bulk of the spectrum is dominated by synchrotron emission and the radio luminosity traces the SFR. In the lower panel we present the starburst case, where $\nu_{\text{crit}} \approx 500$ MHz. In this case only observations above ≈ 500 MHz can be employed for estimating the SFR. If the observational frequency is, however, too high, the result might be affected by the contribution of free-free emission. The different colors in Figure 2 refer to different SFRs. As expected from the correlation of the number of cosmic rays, the synchrotron flux decreases with decreasing \dot{M}_\star .

In Figure 3 the radio luminosities at different fixed frequencies are plotted as a function of the SFR. With 200 MHz, 500 MHz, and 1.4 GHz, we present typical frequencies used in radio observations. Below $10 \text{ M}_\odot \text{ yr}^{-1}$ we use our model for normal disk galaxies, at higher SFRs the starburst model. The results from the fiducial model are shown as black solid lines. For normal galaxies the full parameter range results in a scaling of the radio luminosity with \dot{M}_\star . This can be expected, as in this case all the exemplary frequencies are higher than ν_{crit} (see Figure 1). At 200 MHz (upper panel of Figure 3) and observations of starbursts, non-thermal radio emission can only be used for extremely low gas densities. For a large range of the parameter space, no correlation with \dot{M}_\star is expected. Observations at 500 MHz (middle panel of Figure 3) are close to the critical frequency for starbursts. Here synchrotron emission already becomes suppressed, but a correlation with star formation is still present for a large range of the parameter space. At 1.4 GHz (lower panel of Figure 3) the SFR estimate via radio emission is possible for the full range of parameters studied in this paper.

Based on these findings we provide the following fitting formulae for our fiducial value of the Milky Way like galaxy at different observing frequencies:

$$\frac{\dot{M}_\star}{\text{M}_\odot \text{ yr}^{-1}} \approx \begin{cases} 3.20 \times 10^{-5} \frac{60 \text{ MHz } L_{60 \text{ MHz}}}{L_\odot} \\ 2.29 \times 10^{-5} \frac{200 \text{ MHz } L_{200 \text{ MHz}}}{L_\odot} \\ 1.63 \times 10^{-5} \frac{1.4 \text{ GHz } L_{1.4 \text{ GHz}}}{L_\odot} \end{cases} \quad (21)$$

For the fiducial model of starburst cores, we only find a correlation between the SFR and the non-thermal radio luminosity for high frequencies. A fit to the M 82 case yields the following formula:

$$\frac{\dot{M}_\star}{\text{M}_\odot \text{ yr}^{-1}} \approx 1.39 \times 10^{-4} \frac{1.4 \text{ GHz } L_{1.4 \text{ GHz}}}{L_\odot}. \quad (22)$$

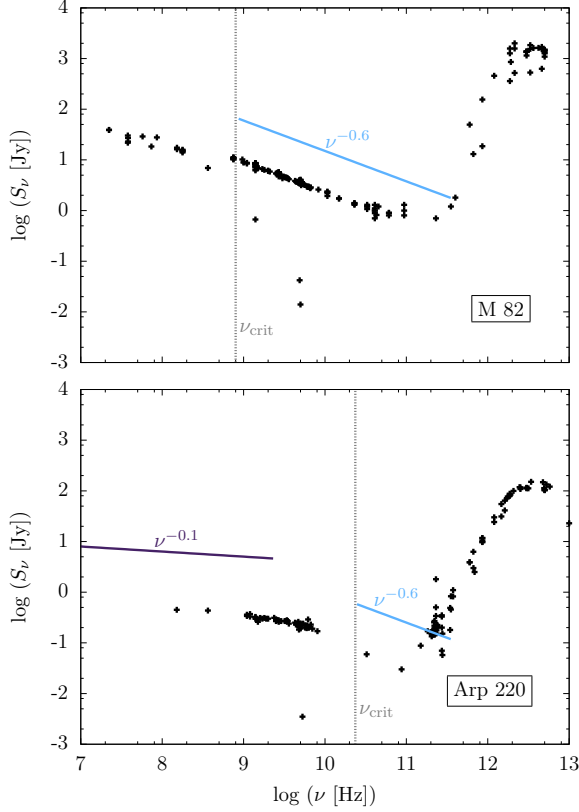


Figure 4. The observed spectra of two exemplary starburst galaxies: M 82 in the top panel and Arp 220 in the lower panel. The black dots show the photometric data from the *NASA/IPAC Extragalactic Database*^a (NED). In the radio regime we indicate the scaling that results from free-free emission ($S_\nu \propto \nu^{-0.1}$) and the scaling expected from synchrotron emission ($S_\nu \propto \nu^{-(\chi-1)/2}$, i.e. $S_\nu \propto \nu^{-0.6}$ for our power law exponent of $\chi = 2.2$). The critical frequency below which the gas becomes optically thick, ν_{crit} is presented as the vertical dotted grey line.

^a<https://ned.ipac.caltech.edu/>

The fitting functions (21) and (22) from our model can be compared the SFR calibrator reported in Murphy *et al.* (2011). These authors estimate the relation between the SFR and the integrated IR flux using Starburst99 (Leitherer *et al.* 1999). By combining this result with the empirical FIR-radio correlation they find the following correlation:

$$\frac{\dot{M}_\star}{M_\odot \text{ yr}^{-1}} \approx 1.74 \times 10^{-4} \frac{1.4 \text{ GHz } L_{1.4 \text{ GHz}}}{L_\odot}. \quad (23)$$

The proportionality factor is close to the one found for our fiducial starburst case.

3.3. Application to local galaxies

In this section, we apply our model to exemplary local galaxies for which the SFR can also be estimated from traditional tracers. We choose the gas-rich disk galaxy M 51, the core of M 82, which is also our fiducial model for starburst galaxies, and the core region of Arp 220. The input parameters are listed in Table 2. Most of the free parameters are constrained from observations. We test our model for radio observations at 1.4 GHz and 1.5 GHz which is typically above the critical frequency for synchrotron absorption (see e.g. Figure 1). The critical

frequency ν_{crit} can be calculated from equation (16). For M 51 and M 82 the critical frequencies are 9.8×10^6 Hz and 8.7×10^8 Hz, respectively, and so synchrotron emission is not suppressed by free-free absorption at 1.4 GHz. The density of Arp 220 is roughly four times higher than the one of M 82, and therefore ν_{crit} reaches a value of 2.36×10^{10} Hz, which exceeds an observing frequency of 1.4 GHz.

The observed radio spectra presented in Figure 4 indicate the suppression of synchrotron emission below ν_{crit} . The flux density S_ν is related to the luminosity via $\nu L_\nu = \nu S_\nu 4\pi d^2$ where d is the distance of the source. For M 82 the flux density above ν_{crit} scales with approximately $\nu^{-(\chi-1)/2}$ which is $\nu^{-0.6}$ for a scaling of the cosmic ray spectrum with $\chi = 2.2$. This is expected for synchrotron emission. At frequencies above a few times 10^{11} Hz, the spectrum is dominated by thermal emission. The critical frequency, which is indicated as a dashed gray line, is much higher in the case of Arp 220. Here synchrotron emission is suppressed by free-free absorption. At an observing frequency of 1.4 GHz our model for estimating the SFR should not be used. There are not many photometric data points above ν_{crit} and below the thermal peak for Arp 220. This makes this galaxy unsuitable for our method. We note that the scaling of the spectrum at low frequencies is roughly proportional to $\nu^{-0.1}$. This could be an indication of free-free emission from the halo along the line of sight, in which the gas density is lower and thus the gas is less optically thick.

In Table 2 the estimates for the star formation rate of the different galaxies are listed. We present the results for $\dot{M}_\star^{1.4 \text{ GHz}}$ and $\dot{M}_\star^{1.5 \text{ GHz}}$ for using our full model, i.e. calculating the cosmic ray spectrum and the free-free processes with the set of observational parameters. In addition we present the result for the SFR when using the observed luminosities and the fitting formulas as given in (21) and (22).

For comparison we determine the SFR also from commonly used tracer, namely the FIR emission which is thermal emission of dust that has been heated via UV radiation from massive stars. Kennicutt (1998) suggests the following scaling of \dot{M}_\star with the FIR luminosity L_{FIR}

$$L_{\text{FIR}} = 5.79 \times 10^9 L_\odot \frac{\dot{M}_\star}{M_\odot \text{ yr}^{-1}}. \quad (24)$$

The FIR luminosity equals roughly 1.7 times the luminosity at $60 \mu\text{m}$ (Chapman *et al.* 2000). Hence, the SFR can be estimated as

$$\dot{M}_\star^{60 \mu\text{m}} = \frac{60 \mu\text{m } L_{60 \mu\text{m}}}{L_\odot} \frac{M_\odot \text{ yr}^{-1}}{1.7 \times 5.79 \times 10^9}. \quad (25)$$

In addition we compare to the SFR calibration at $70 \mu\text{m}$ (Calzetti *et al.* 2010):

$$\frac{\dot{M}_\star^{70 \mu\text{m}}}{M_\odot \text{ yr}^{-1}} \approx 2.26 \times 10^{-10} \frac{c L_{70 \mu\text{m}}}{70 \mu\text{m } L_\odot} \quad (26)$$

Table 2
Comparison of our model with other SFR tracers

	M 51	M 82	Apr 220
input:			
n [cm ⁻³]	5 (Koda <i>et al.</i> 2009)	300 (Weiß <i>et al.</i> 2001)	10 ⁴ (Anantharamaiah <i>et al.</i> 2000)
T_e [K]	10 ⁴	5 × 10 ³	7500 (Anantharamaiah <i>et al.</i> 2000)
H [pc]	150 (Hu <i>et al.</i> 2013)	200 (Adebahr <i>et al.</i> 2013)	1000 (Anantharamaiah <i>et al.</i> 2000)
f_{ion}	0.1	0.1	0.1
L_{fill}	0.2	0.2	-
B [G]	2 × 10 ⁻⁵ (Fletcher <i>et al.</i> 2011)	5 × 10 ⁻⁵ (Klein <i>et al.</i> 1988)	-
u_{int} [erg cm ⁻³]	10 ⁻¹²	10 ⁻⁹	-
v_{wind} [km s ⁻¹]	50	230 (Walter <i>et al.</i> 2002)	-
ΔA [cm ²]	10 ⁴³	10 ⁴¹	-
d [pc]	7.97 × 10 ⁶ (mean from NED)	3.93 × 10 ⁶ (mean from NED)	7.72 × 10 ⁷ (mean from NED)
observed fluxes:			
$S_{1.4 \text{ GHz}}$ [Jy]	1.4 (Dumas <i>et al.</i> 2011)	8.67 (Pauliny-Toth <i>et al.</i> 1966)	0.326 (Condon <i>et al.</i> 2002)
$S_{1.5 \text{ GHz}}$ [Jy]	8.1 (Mulcahy <i>et al.</i> 2014)	6.85 (Williams and Bower 2010)	0.26 (Williams and Bower 2010)
$S_{70 \mu\text{m}}$ [Jy]	-	1630 (Dale <i>et al.</i> 2009)	-
$S_{60 \mu\text{m}}$ [Jy]	70.3 (Tuffs and Gabriel 2003)	1313.46 (Soifer <i>et al.</i> 1989)	103.33 (Soifer <i>et al.</i> 1989)
$S_{24 \mu\text{m}}$ [Jy]	-	325 (Dale <i>et al.</i> 2009)	5.57 (Brown <i>et al.</i> 2014)
SFR from our model:			
ν_{crit} [Hz] ^a	9.8 × 10 ⁶	8.73 × 10 ⁸	2.36 × 10 ¹⁰
$\dot{M}_{\star}^{1.4 \text{ GHz}}$ [$M_{\odot}\text{yr}^{-1}$] ^b	0.60	8.14	-
$\dot{M}_{\star}^{1.5 \text{ GHz}}$ [$M_{\odot}\text{yr}^{-1}$] ^c	0.63	8.13	(118)
$\dot{M}_{\star}^{1.5 \text{ GHz}}$ [$M_{\odot}\text{yr}^{-1}$] ^d	3.65	6.39	-
SFR from other tracers:			
$\dot{M}_{\star}^{1.4 \text{ GHz}}$ [$M_{\odot}\text{yr}^{-1}$] ^e	6.72	10.12	146
$\dot{M}_{\star}^{70 \mu\text{m}}$ [$M_{\odot}\text{yr}^{-1}$] ^f	-	7.64	-
$\dot{M}_{\star}^{60 \mu\text{m}}$ [$M_{\odot}\text{yr}^{-1}$] ^g	2.04	9.29	281
$\dot{M}_{\star}^{24 \mu\text{m}}$ [$M_{\odot}\text{yr}^{-1}$] ^h	-	15.34	101

Note. — Testing our model for exemplary galaxies. We list the input parameters, the observed fluxes, and the estimate of the SFR from our model. In brackets we give the estimate from our fitting formulas (21) or (22), respectively. For comparison we list the SFRs resulting from traditional calibrations: $\dot{M}_{\star}^{1.4 \text{ GHz}}$ (Murphy *et al.* 2011), $\dot{M}_{\star}^{24 \mu\text{m}}$ (Rieke *et al.* 2009), $\dot{M}_{\star}^{60 \mu\text{m}}$ (Chapman *et al.* 2000), $\dot{M}_{\star}^{70 \mu\text{m}}$ (Calzetti *et al.* 2010).

^ausing equation (16)

^bfull model

^cusing fitting formulas (21) and (22)

^dfull model

^eMurphy *et al.* (2011): $\dot{M}_{\star}^{1.4 \text{ GHz}}/(M_{\odot} \text{ yr}^{-1}) \approx 1.74 \times 10^{-4} \text{ } 1.4 \text{ GHz } L_{1.4 \text{ GHz}}/L_{\odot}$

^fCalzetti *et al.* (2010): $\dot{M}_{\star}^{70 \mu\text{m}}/(M_{\odot} \text{ yr}^{-1}) \approx 2.26 \times 10^{-10} \text{ } c \text{ } L_{70\mu\text{m}}/(70\mu\text{m } L_{\odot})$

^gChapman *et al.* (2000): $\dot{M}_{\star}^{60 \mu\text{m}}/(M_{\odot} \text{ yr}^{-1}) \approx 2.94 \times 10^{-10} \text{ } c \text{ } L_{60\mu\text{m}}/(60\mu\text{m } L_{\odot})$

^hRieke *et al.* (2009): $\dot{M}_{\star}^{24 \mu\text{m}}/(M_{\odot} \text{ yr}^{-1}) \approx 7.84 \times 10^{-10} \text{ } c \text{ } L_{24\mu\text{m}}/(24\mu\text{m } L_{\odot})$

and at 24 μm (Rieke *et al.* 2009)³:

$$\frac{\dot{M}_{\star}^{24 \mu\text{m}}}{M_{\odot} \text{ yr}^{-1}} \approx 7.84 \times 10^{-10} \frac{c \text{ } L_{24\mu\text{m}}}{24\mu\text{m } L_{\odot}}. \quad (27)$$

Moreover, we list the SFR estimate from the empirical 1.4 GHz calibration suggested by Murphy *et al.* (2011) (see equation 23).

For the case of M 51 our model yields $\dot{M}_{\star}^{1.4 \text{ GHz}} = 0.6 M_{\odot}\text{yr}^{-1}$, both for the full calculation and the fitting formula, and $\dot{M}_{\star}^{1.5 \text{ GHz}} = 3.65 M_{\odot}\text{yr}^{-1}$. These values are comparable to the one from the 60 μm emission, which yields $\dot{M}_{\star}^{60 \mu\text{m}} = 2.04 M_{\odot}\text{yr}^{-1}$. The calibration by Murphy *et al.* (2011) results into a slightly higher value of $6.72 M_{\odot}\text{yr}^{-1}$. Also for M 82, which is our fiducial star-

burst galaxy, our estimates, $\dot{M}_{\star}^{1.4 \text{ GHz}} = 8.14 M_{\odot}\text{yr}^{-1}$ and $\dot{M}_{\star}^{1.5 \text{ GHz}} = 6.39 M_{\odot}\text{yr}^{-1}$, are in agreement with the calibrations from literature. As mentioned before, Arp 220 is not a good candidate for the SFR estimate presented in this paper. Because of the high value of ν_{crit} , synchrotron emission is suppressed at 1.4 GHz and thus we expect no correlation with star formation at this frequency. Ignoring this condition and estimating the SFR with the 1.4 GHz flux results into $118 M_{\odot}\text{yr}^{-1}$ which is about a factor of three smaller than the estimate via the 60 μm emission and comparable to the one from the 24 μm emission. The deviations can, however, be larger depending on the contribution from free-free and thermal emission. In general, our physical model for the relation between radio emission and the SFR coincides well with traditional SFR tracers.

³ We note that the luminosities with an index, e.g. $L_{70\mu\text{m}}$ and $L_{24\mu\text{m}}$ are spectral luminosities with the units erg/(s Hz). These need to be multiplied with the observing frequencies $c/70\mu\text{m}$ and $c/24\mu\text{m}$, respectively, to gain the physical luminosities with the units erg/s.

4. OBSERVATIONS OF HIGHLY REDSHIFTED GALAXIES

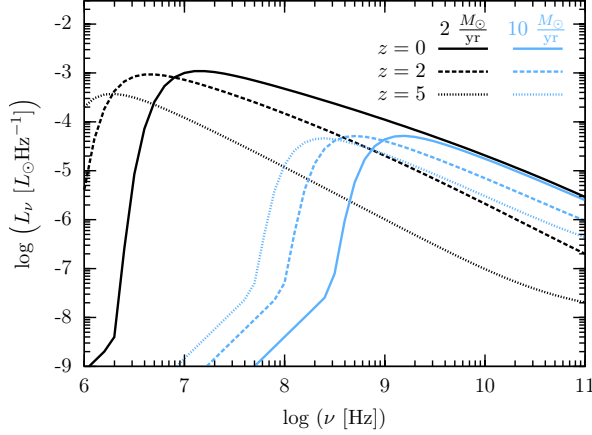


Figure 5. The spectral total radio luminosity L_ν for our fiducial model of the Milky Way (black lines) and M 82 (blue lines). Different line types correspond to different redshifts z .

An important goal of the upcoming radio telescopes is to study galaxies at early times and their evolution to the present day. Theory predicts young galaxies to be smaller and denser and to have higher star formation rates than their local counterparts. Observations at high redshifts are crucial to constrain theories of evolution of galaxies and galactic star formation.

Hypothetically, when moving a galaxy of fixed density and star formation rate to higher redshift, one expects two effects on the resulting radio luminosity. First, the number of cosmic rays is reduced, as they lose energy faster via inverse Compton scattering with the stronger CMB. This results in less synchrotron emission and thus needs to be taken into account when estimating the SFR. Second, spectral signatures, like the critical frequency, move to smaller ν in the observed frame. In fact the critical frequency in the observed frame is

$$\frac{\nu_{\text{crit,obs}}}{10^9 \text{ Hz}} = \frac{1}{1+z} \left(0.082 \left(\frac{T_e}{\text{K}} \right)^{-1.35} \left(\frac{EM(n)}{\text{cm}^{-6} \text{ pc}} \right) \right)^{1/2.1}. \quad (28)$$

Consequently, non-thermal radio emission from highly redshifted galaxies can be used also at lower frequencies.

Figure 5 shows how the spectra change with increasing redshift for the Milky Way model (black lines) and the M 82 model (blue lines). The critical frequency, i.e. the turnover of the spectrum, shifts to smaller ν as z increases. For our fiducial starburst galaxy non-thermal radio emission cannot be employed as a SFR tracer at 60 MHz and $z = 0$, while it becomes possible again at the same ν and $z = 5$. For the starburst case, the normalization of the spectrum is not affected significantly by higher redshift, as the intrinsic radiation is very strong compared to the CMB, also at $z = 5$. Similarly, Figure 6 presents how ν_{crit} decreases with increasing redshift. Hence, a galaxy which is no candidate for our method in the local Universe, can show a correlation between the SFR and the non-thermal radio emission if it was at higher redshift. This is blueillustrated in Figure 7 where we show how the correlation of radio luminosity at different fixed observed frequencies is reestablished as z increases. We note here, that the total radio lumi-

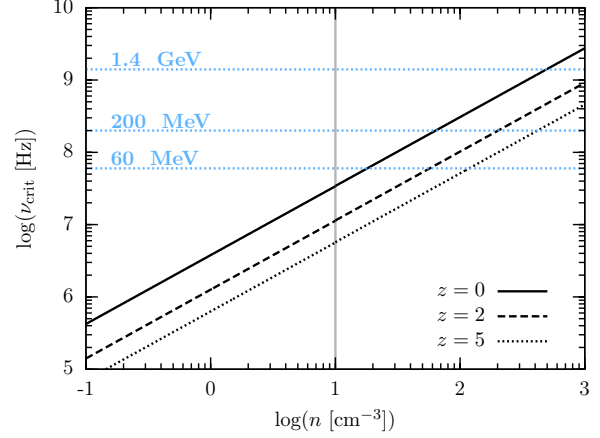


Figure 6. The critical frequency ν_{crit} below which the optical depth $\tau_{\text{ff}} < 1$ as a function of the gas density n . We present the result for the fiducial galaxies at different redshifts z .

nosity decreases with z , as the number of cosmic rays is reduced by stronger inverse Compton losses. This effect is less important for starbursts, as they host a very strong intrinsic interstellar radiation field, which is much stronger than the CMB up to high redshifts.

Detailed observations of highly redshifted galaxies are possible if they are gravitationally lensed by massive foreground galaxy clusters. For example, Ivison *et al.* (2010) estimate the properties of SMM J21350102, also known as the cosmic eyelash, which has a redshift of $z = 2.3$. They report a density of $n = 10^3 \text{ cm}^{-3}$. Assuming a scale height of 100 pc, which is based on an estimate of the galaxies star forming regions (Swinbank *et al.* 2010), an electron temperature of $T_e = 5000 \text{ K}$, $f_{\text{ion}} = 0.1$, and $f_{\text{fill}} = 0.2$, we find a critical frequency of $\nu_{\text{crit}} = 5.94 \times 10^8 \text{ Hz}$. Inserting a spectral radio luminosity of $L_{1.4 \text{ GHz}} = 9 \times 10^{23} \text{ W Hz}^{-1}$ (Ivison *et al.* 2010) into the fitting formula (22) yields a SFR of $456 M_\odot \text{ yr}^{-1}$. This is comparable to the estimate of $400 M_\odot \text{ yr}^{-1}$ based on the intrinsic rest-frame 8-1000 μm luminosity (Ivison *et al.* 2010).

One potential caveat for using radio emission to study star formation at high redshift, is that in future deep surveys also a large number of active galactic nuclei (AGNs) will be seen. They can dominate the radio regime and will make it impossible to estimate the star formation rate of their host galaxies. Galaxies hosting an AGN can be excluded from the data set by identifying them with X-ray observations (Treister *et al.* 2009) or by detecting radio jets if the latter can be specially resolved. In addition, the thermal component of the radio spectrum moves to lower frequencies in the rest frame. If the critical frequency is too close to the thermal emission our SFR estimate will not be good.

5. CONCLUSION

In this paper we studied the conditions under which non-thermal radio emission can be used to estimate the star formation rate. The underlying physical connection between the two quantities are cosmic rays, which are produced in supernova shock fronts and thus are linked to a galaxy's SFR. These high-energy charged particles emit synchrotron radiation when traveling through the

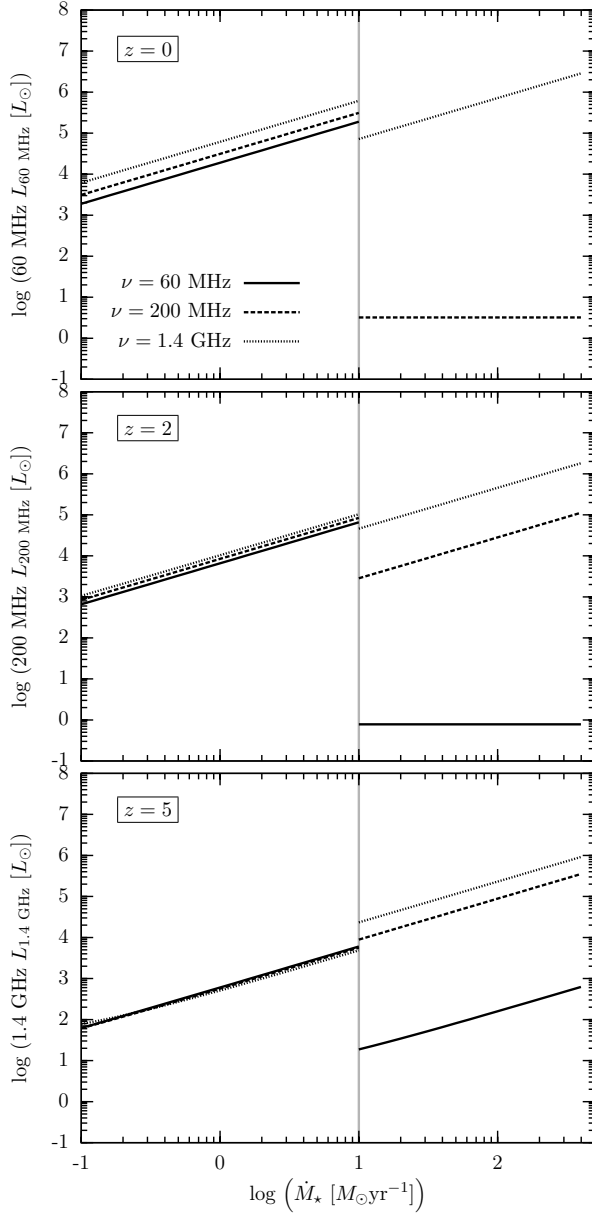


Figure 7. A test of the correlation between radio luminosity νL_ν and the star formation rate \dot{M}_\odot . We explore different observed frequencies and the luminosity at redshift $z = 0$ (black lines), $z = 2$ (blue lines), and $z = 5$ (orange lines). Except for z and \dot{M}_\odot all free parameters used here are for the fiducial galaxies.

magnetized interstellar medium. Here we have derived an estimate of the galactic radio luminosity as a function of the SFR. The main results of this work are:

- Synchrotron emission is proportional to the star formation rate. The main dependency results from the production of cosmic rays which takes place in supernova shock fronts and is thus related to the supernova rate, which in turn scales as the SFR.
- If the gas density is too high, however, synchrotron emission is absorbed by the free-free process. This absorption is especially important at low frequencies. In fact, below a critical frequency ν_{crit} (see equation 16) radio emission cannot be employed

for measuring SFRs at very low frequencies.

- At high redshifts, the observed radio spectrum and with it the critical frequency moves to lower frequencies (see equation 28). Here radio emission can again be used to determine SFRs also for dense young galaxies.
- The relation between SFR and radio luminosity at different frequencies is described by equation (18). In addition, we provide simply fitting formulae for normal disk galaxies and starburst systems in equations (21) and (22).

Our method should be a useful tool for future deep radio surveys, for example with the SKA. Most surveys will be performed at a fixed observing frequency. Without the information from the spectral flux distribution, special caution is required. First of all, the critical frequency ν_{crit} should be estimated, see equation (16) for local observations and equation (28) for the high- z case. Our estimate for the SFR should only be applied if the observing frequency is above ν_{crit} . Otherwise the synchrotron emission is absorbed and the radio flux is not correlated with the SFR. The latter can then be estimated with the fitting formulas given in equations (21) for normal disk galaxies and in equation (22) for starbursts.

We note however, that our model includes several free parameters which are summarized in Table 1. While the fitting formulas given in equations (21) and (22) are for our fiducial cases, the accuracy can be increased if additional parameters of the galaxy, like the gas density and the scale height, are known. Additionally, the thermal and the free-free contribution might be important especially at higher radio frequencies, or at even at lower frequencies if the spectrum is highly redshifted. The latter contributions depend on the galaxy’s temperature and surface area. For example, the thermal peak in the spectrum of the starburst galaxy Arp 220 occurs above approximately 100 GHz (see Figure 4). In the observed spectrum of a similar galaxy at $z = 10$, the flux would be thermally dominated already at frequencies of 9 GHz. Additionally, the presence of an AGN should be excluded, which could easily dominate the galactic radio emission. We have applied our method to first exemplary test galaxies which are presented in Table 2. The SFRs determined from non-thermal radio emission are comparable the ones resulting from the FIR flux which is a more traditional tracer of star formation.

This work has been financially supported by *Nordita* which is funded by the Nordic Council of Ministers, the Swedish Research Council, and the two host universities, the *Royal Institute of Technology (KTH)* and *Stockholm University*. DRGS thanks for funding through Fondecyt regular (project code 1161247), through the “Concurso Proyectos Internacionales de Investigación, Convocatoria 2015” (project code PII20150171), and from the Chilean BASAL Centro de Excelencia en Astrofísica y Tecnologías Afines (CATA) grant PFB-06/2007. We further thank for funding through the *Deutsche Forschungsgemeinschaft (DFG)* in the *Schwerpunktprogramm SPP 1573 “Physics of the Interstellar Medium”* under grants

KL 1358/14-1, SCHL 1964/1-1, SCHL 1964/1-2, and BO 4113/1-2. In addition we thank the DFG for support via the SFB 881 “The Milky Way System” in the sub-projects B1 and B2. Also we acknowledge financial support by the *European Research Council* under the *European Community’s Seventh Framework Programme* (FP7/2007-2013) via the ERC *Advanced Grant* STARLIGHT (project number 339177).

REFERENCES

- V. Bromm and N. Yoshida, *ARA&A* **49**, 373 (2011).
C. J. Conselice, *ARA&A* **52**, 291 (2014).
P. Madau and M. Dickinson, *ARA&A* **52**, 415 (2014).
R. S. Somerville and R. Davé, *ARA&A* **53**, 51 (2015).
J. H. Wise, M. J. Turk, and T. Abel, *ApJ* **682**, 745 (2008).
T. H. Greif, J. L. Johnson, R. S. Klessen, and V. Bromm, *MNRAS* **387**, 1021 (2008).
D. Ceverino and A. Klypin, *ApJ* **695**, 292 (2009).
R. G. Bower, A. J. Benson, R. Malbon, J. C. Helly, C. S. Frenk, C. M. Baugh, S. Cole, and C. G. Lacey, *MNRAS* **370**, 645 (2006).
P. F. Hopkins, P. Torrey, C.-A. Faucher-Giguère, E. Quataert, and N. Murray, *MNRAS* **458**, 816 (2016).
J. M. Lotz, M. Davis, S. M. Faber, P. Guhathakurta, S. Gwyn, J. Huang, D. C. Koo, E. Le Floch, L. Lin, J. Newman, K. Noeske, C. Papovich, C. N. A. Willmer, A. Coil, C. J. Conselice, M. Cooper, A. M. Hopkins, A. Metevier, J. Primack, G. Rieke, and B. J. Weiner, *ApJ* **672**, 177 (2008).
R. Pakmor and V. Springel, *MNRAS* **432**, 176 (2013).
R. J. Bouwens, G. D. Illingworth, P. A. Oesch, M. Stiavelli, P. van Dokkum, M. Trenti, D. Magee, I. Labbé, M. Franx, C. M. Carollo, and V. Gonzalez, *ApJ* **709**, L133 (2010).
R. J. McLure, J. S. Dunlop, M. Cirasuolo, A. M. Koekemoer, E. Sabbi, D. P. Stark, T. A. Targett, and R. S. Ellis, *MNRAS* **403**, 960 (2010).
R. J. Bouwens, G. D. Illingworth, I. Labbe, P. A. Oesch, M. Trenti, C. M. Carollo, P. G. van Dokkum, M. Franx, M. Stiavelli, V. González, D. Magee, and L. Bradley, *Nature* **469**, 504 (2011).
R. J. Ivison, A. M. Swinbank, B. Swinyard, I. Smail, C. P. Pearson, D. Rigopoulou, E. Polehampton, J.-P. Baluteau, M. J. Barlow, A. W. Blain, J. Bock, D. L. Clements, K. Coppin, A. Cooray, A. Danielson, E. Dwek, A. C. Edge, A. Franceschini, T. Fulton, J. Glenn, M. Griffin, K. Isaak, S. Leeks, T. Lim, D. Naylor, S. J. Oliver, M. J. Page, I. Pérez Fournon, M. Rowan-Robinson, G. Savini, D. Scott, L. Spencer, I. Valtchanov, L. Vigroux, and G. S. Wright, *A&A* **518** (2010).
M. A. Garrett, *A&A* **384**, L19 (2002).
C. Gruppioni, F. Pozzi, G. Zamorani, P. Ciliegi, C. Lari, E. Calabrese, F. La Franca, and I. Matute, *MNRAS* **341**, L1 (2003).
P. N. Appleton, D. T. Fadda, F. R. Marleau, D. T. Frayer, G. Helou, J. J. Condon, P. I. Choi, L. Yan, M. Lacy, G. Wilson, L. Armus, S. C. Chapman, F. Fang, I. Heinrichson, M. Im, B. T. Jannuzi, L. J. Storrie-Lombardi, D. Shupe, B. T. Soifer, G. Squires, and H. I. Teplitz, *ApJS* **154**, 147 (2004).
M. J. Jarvis, D. J. B. Smith, D. G. Bonfield, M. J. Hardcastle, J. T. Falder, J. A. Stevens, R. J. Ivison, R. Auld, M. Baes, I. K. Baldry, S. P. Bamford, N. Bourne, S. Buttiglione, A. Cava, A. Cooray, A. Dariush, G. de Zotti, J. S. Dunlop, L. Dunne, S. Dye, S. Eales, J. Fritz, D. T. Hill, R. Hopwood, D. H. Hughes, E. Ibar, D. H. Jones, L. Kelvin, A. Lawrence, L. Leeuw, J. Loveday, S. J. Maddox, M. J. Michałowski, M. Negrello, P. Norberg, M. Pohlen, M. Prescott, E. E. Rigby, A. Robotham, G. Rodighiero, D. Scott, R. Sharp, P. Temi, M. A. Thompson, P. van der Werf, E. van Kampen, C. Vlahakis, and G. White, *MNRAS* **409**, 92 (2010).
M. T. Sargent, E. Schinnerer, E. Murphy, C. L. Carilli, G. Helou, H. Aussel, E. Le Floch, D. T. Frayer, O. Ilbert, P. Oesch, M. Salvato, V. Smolčić, J. Kartaltepe, and D. B. Sanders, *ApJ* **714**, L190 (2010).
N. Bourne, L. Dunne, R. J. Ivison, S. J. Maddox, M. Dickinson, and D. T. Frayer, *MNRAS* **410**, 1155 (2011).
G. R. Blumenthal and R. J. Gould, *Reviews of Modern Physics* **42**, 237 (1970).
M. S. Longair, *High Energy Astrophysics*, by Malcolm S. Longair, Cambridge, UK: Cambridge University Press, 2011 (2011).
A. R. Bell, *MNRAS* **182**, 147 (1978a).
A. R. Bell, *MNRAS* **182**, 443 (1978b).
L. Drury, *Space Sci. Rev.* **36**, 57 (1983).
R. Schlickeiser, *Cosmic ray astrophysics / Reinhard Schlickeiser, Astronomy and Astrophysics Library; Physics and Astronomy Online Library. Berlin: Springer. ISBN 3-540-66465-3, 2002, XV + 519 pp.* (2002).
J. J. Condon, *ARA&A* **30**, 575 (1992).
S. Niklas and R. Beck, *A&A* **320**, 54 (1997).
M. S. Yun, N. A. Reddy, and J. J. Condon, *ApJ* **554**, 803 (2001).
E. F. Bell, *ApJ* **586**, 794 (2003).
B. A. Groves, J. Cho, M. Dopita, and A. Lazarian, *Pub. of the Astron. Soc. of Australia* **20**, 252 (2003).
B. C. Lacki, T. A. Thompson, and E. Quataert, *ApJ* **717**, 1 (2010).
B. C. Lacki and T. A. Thompson, *ApJ* **717**, 196 (2010).
D. R. G. Schleicher and R. Beck, *A&A* **556**, A142 (2013).
D. R. G. Schleicher and R. Beck, *A&A* **593**, A77 (2016).
J. Schöber, D. R. G. Schleicher, and R. S. Klessen, *ApJ* **827**, 109 (2016).
C.-N. Hao, R. C. Kennicutt, B. D. Johnson, D. Calzetti, D. A. Dale, and J. Moustakas, *ApJ* **741**, 124 (2011).
E. J. Murphy, J. J. Condon, E. Schinnerer, R. C. Kennicutt, D. Calzetti, L. Armus, G. Helou, J. L. Turner, G. Aniano, P. Beirão, A. D. Bolatto, B. R. Brandl, K. V. Croxall, D. A. Dale, J. L. Donovan Meyer, B. T. Draine, C. Engelbracht, L. K. Hunt, C.-N. Hao, J. Koda, H. Roussel, R. Skibba, and J.-D. T. Smith, *ApJ* **737**, 67 (2011).
R. C. Kennicutt and N. J. Evans, *ARA&A* **50**, 531 (2012).
P. Madau, L. Pozzetti, and M. Dickinson, *ApJ* **498**, 106 (1998).
A. M. Hillas, *ArXiv Astrophysics e-prints* (2006), astro-ph/0607109.
T. J. Bogdan and H. J. Völk, *A&A* **122**, 129 (1983).
B. C. Lacki and R. Beck, *MNRAS* **430**, 3171 (2013).
E. A. Dorfi, *Ap&SS* **272**, 227 (2000).
M. Ehle and R. Beck, *A&A* **273**, 45 (1993).
E. M. Berkhuijsen, D. Mitra, and P. Mueller, *Astronomische Nachrichten* **327** (2006), 10.1002/asna.200510488, astro-ph/0511172.
R. Beck, *A&A* **470**, 539 (2007).
R. Beck, *A&A Rev.* **24**, 4 (2016).
A. Fletcher, in *The Dynamic Interstellar Medium: A Celebration of the Canadian Galactic Plane Survey*, Astronomical Society of the Pacific Conference Series, Vol. 438, edited by R. Kothés, T. L. Landecker, and A. G. Willis (2010) p. 197.
K. T. Chyży and R. Beck, *A&A* **417** (2004), 10.1051/0004-6361:20031778.
R. Beck, A. Fletcher, A. Shukurov, A. Snodin, D. D. Sokoloff, M. Ehle, D. Moss, and V. Shoutenkov, *A&A* **444**, 739 (2005).
V. Heesen, R. Beck, M. Krause, and R.-J. Dettmar, *A&A* **535**, A79 (2011).
B. Adebahr, M. Krause, U. Klein, M. Weżgowiec, D. J. Bomans, and R.-J. Dettmar, *A&A* **555**, A23 (2013).
P. Kroupa, *Science* **295**, 82 (2002).
P. M. W. Kalberla and L. Dedes, *A&A* **487**, 951 (2008).
J. W. Colbert, M. A. Malkan, P. E. Clegg, P. Cox, J. Fischer, S. D. Lord, M. Luhman, S. Satyapal, H. A. Smith, L. Spinoglio, G. Stacey, and S. J. Unger, *ApJ* **511** (1999), 10.1086/306711.
B. T. Draine, *Physics of the Interstellar and Intergalactic Medium by Bruce T. Draine. Princeton University Press, 2011. ISBN: 978-0-691-12214-4* (2011).
M. Kregel, P. C. van der Kruit, and R. de Grijs, *MNRAS* **334** (2002), 10.1046/j.1365-8711.2002.05556.x.
H.-W. Rix and J. Bovy, *A&A Rev.* **21**, 61 (2013).
E. de Cea del Pozo, D. F. Torres, and A. Y. Rodríguez Marrero, *ApJ* **698**, 1054 (2009).
P. Girichidis, S. Walch, T. Naab, A. Gatto, R. Wünsch, S. C. O. Glover, R. S. Klessen, P. C. Clark, T. Peters, D. Derigs, and C. Baczynski, *MNRAS* **456**, 3432 (2016).
F. Walter, A. Weiss, and N. Scoville, *ApJ* **580**, L21 (2002).
C. Quireza, R. T. Rood, T. M. Bania, D. S. Balser, and W. J. Maciel, *ApJ* **653** (2006), 10.1086/508803, astro-ph/0609006.
P. J. Puxley, P. W. J. L. Brand, T. J. T. Moore, C. M. Mountain, N. Nakai, and T. Yamashita, *ApJ* **345** (1989), 10.1086/167891.
A. G. G. M. Tielens, *The Physics and Chemistry of the Interstellar Medium* (Cambridge University Press, 2005).
C. Leitherer, D. Schaerer, J. D. Goldader, R. M. G. Delgado, C. Robert, D. F. Kune, D. F. de Mello, D. Devost, and T. M. Heckman, *ApJS* **123**, 3 (1999).
J. Koda, N. Scoville, T. Sawada, M. A. La Vigne, S. N. Vogel, A. E. Potts, J. M. Carpenter, S. A. Corder, M. C. H. Wright, S. M. White, B. A. Zauderer, J. Patience, A. I. Sargent, D. C. J. Bock, D. Hawkins, M. Hodges, A. Kemball, J. W. Lamb, R. L. Plambeck, M. W. Pound, S. L. Scott, P. Teuben, and D. P. Woody, *ApJ* **700**, L132 (2009).

- A. Weiß, N. Neininger, S. Hüttemeister, and U. Klein, *A&A* **365**, 571 (2001), astro-ph/0010541.
- K. R. Anantharamaiah, F. Viallefond, N. R. Mohan, W. M. Goss, and J. H. Zhao, *ApJ* **537**, 613 (2000), astro-ph/0004293.
- T. Hu, Z. Shao, and Q. Peng, *ApJ* **762**, L27 (2013).
- A. Fletcher, R. Beck, A. Shukurov, E. M. Berkhuijsen, and C. Horellou, *MNRAS* **412**, 2396 (2011).
- U. Klein, R. Wielebinski, and H. W. Morsi, *A&A* **190**, 41 (1988).
- G. Dumas, E. Schinnerer, F. S. Tabatabaei, R. Beck, T. Velusamy, and E. Murphy, *AJ* **141**, 41 (2011).
- I. I. K. Pauliny-Toth, C. M. Wade, and D. S. Heeschen, *ApJS* **13**, 65 (1966).
- J. J. Condon, W. D. Cotton, and J. J. Broderick, *AJ* **124**, 675 (2002).
- D. D. Mulcahy, A. Horneffer, R. Beck, G. Heald, A. Fletcher, A. Scaife, B. Adebahr, J. M. Anderson, A. Bonafede, M. Brügger, G. Brunetti, K. T. Chyży, J. Conway, R.-J. Dettmar, T. Enßlin, M. Haverkorn, C. Horellou, M. Iacobelli, F. P. Israel, H. Junklewitz, W. Jurusik, J. Köhler, M. Kuniyoshi, E. Orrú, R. Paladino, R. Pizzo, W. Reich, and H. J. A. Röttgering, *A&A* **568**, A74 (2014).
- P. K. G. Williams and G. C. Bower, *ApJ* **710**, 1462 (2010).
- D. A. Dale, S. A. Cohen, L. C. Johnson, M. D. Schuster, D. Calzetti, C. W. Engelbracht, A. Gil de Paz, R. C. Kennicutt, J. C. Lee, A. Begum, M. Block, J. J. Dalcanton, J. G. Funes, K. D. Gordon, B. D. Johnson, A. R. Marble, S. Sakai, E. D. Skillman, L. van Zee, F. Walter, D. R. Weisz, B. Williams, S.-Y. Wu, and Y. Wu, *ApJ* **703**, 517 (2009).
- R. J. Tuffs and C. Gabriel, *A&A* **410**, 1075 (2003).
- B. T. Soifer, L. Boehmer, G. Neugebauer, and D. B. Sanders, *AJ* **98**, 766 (1989).
- M. J. I. Brown, J. Moustakas, J.-D. T. Smith, E. da Cunha, T. H. Jarrett, M. Imanishi, L. Armus, B. R. Brandl, and J. E. G. Peek, *ApJS* **212**, 18 (2014).
- D. Calzetti, S.-Y. Wu, S. Hong, R. C. Kennicutt, J. C. Lee, D. A. Dale, C. W. Engelbracht, L. van Zee, B. T. Draine, C.-N. Hao, K. D. Gordon, J. Moustakas, E. J. Murphy, M. Regan, A. Begum, M. Block, J. Dalcanton, J. Funes, A. Gil de Paz, B. Johnson, S. Sakai, E. Skillman, F. Walter, D. Weisz, B. Williams, and Y. Wu, *ApJ* **714**, 1256 (2010).
- S. C. Chapman, D. Scott, C. C. Steidel, C. Borys, M. Halpern, S. L. Morris, K. L. Adelberger, M. Dickinson, M. Giavalisco, and M. Pettini, *MNRAS* **319**, 318 (2000).
- G. H. Rieke, A. Alonso-Herrero, B. J. Weiner, P. G. Pérez-González, M. Blaylock, J. L. Donley, and D. Marcillac, *ApJ* **692**, 556 (2009).
- R. C. Kennicutt, Jr., *ApJ* **498**, 541 (1998).
- A. M. Swinbank, I. Smail, S. Longmore, A. I. Harris, A. J. Baker, C. De Breuck, J. Richard, A. C. Edge, R. J. Ivison, R. Blundell, K. E. K. Coppin, P. Cox, M. Gurwell, L. J. Hainline, M. Krips, A. Lundgren, R. Neri, B. Siana, G. Siringo, D. P. Stark, D. Wilner, and J. D. Younger, *Nature* **464**, 733 (2010).
- E. Treister, C. M. Urry, and S. Virani, *ApJ* **696** (2009), 10.1088/0004-637X/696/1/110